



From endohedral cluster superconductors to approximant phases: Synthesis, crystal and electronic structure, and physical properties of $\text{Mo}_8\text{Ga}_{41-x}\text{Zn}_x$ and $\text{Mo}_7\text{Ga}_{52-x}\text{Zn}_x$

Journal:	<i>Dalton Transactions</i>
Manuscript ID	DT-ART-12-2018-004982.R1
Article Type:	Paper
Date Submitted by the Author:	08-Apr-2019
Complete List of Authors:	Verchenko, Valeriy; Moscow State University, Department of Chemistry; Keemilise ja Bioloogilise Fuusika Instituut, Chemical Physics Zbtsovskii, Alexander; Moscow State University, Department of Chemistry Wei, Zheng; University at Albany, SUNY, Chemistry Tsirlin, Alexander; Max Planck Institute for Chemical Physics of Solids, ; National Institute of Chemical Physics and Biophysics, Dikarev, Evgeny V.; University at Albany, SUNY, Chemistry Shevelkov, Andrei; Moscow State University, Chemistry

Cite this: DOI: 10.1039/xxxxxxxxxx

From endohedral cluster superconductors to approximant phases: Synthesis, crystal and electronic structure, and physical properties of $\text{Mo}_8\text{Ga}_{41-x}\text{Zn}_x$ and $\text{Mo}_7\text{Ga}_{52-x}\text{Zn}_x$ [†]

 Valeriy Yu. Verchenko,^{*a,b} Alexander O. Zubtsovskii,^{a,c} Zheng Wei,^d Alexander A. Tsirlin,^c Evgeny V. Dikarev,^d and Andrei V. Shevelkov^a

 Received Date
 Accepted Date

DOI: 10.1039/xxxxxxxxxx

www.rsc.org/journalname

Using the crystal-growth joint flux technique based on the combination of two aliovalent low-melt metals, gallium and zinc, we adjust the gross valence electron count in the Mo-Ga-Zn system and produce the $\text{Mo}_8\text{Ga}_{41-x}\text{Zn}_x$ and $\text{Mo}_7\text{Ga}_{52-x}\text{Zn}_x$ intermetallic compounds. Gradual reduction in the valence electron count first leads to the Zn for Ga substitution in the $\text{Mo}_8\text{Ga}_{41}$ endohedral cluster superconductor, accompanied by the formation of Zn-containing clusters in the crystal structure and by the gradual suppression of superconductivity. $\text{Mo}_8\text{Ga}_{41-x}\text{Zn}_x$ with $x = 7.2(2)$ exhibits superconducting properties below $T_C = 4$ K, whereas there is no superconducting transition at temperatures above 2 K for the limiting composition of $x = 11.3(2)$. Further, the $\text{Mo}_7\text{Ga}_{52-x}\text{Zn}_x$ phase is formed from the flux with a higher content of Zn. $\text{Mo}_7\text{Ga}_{52-x}\text{Zn}_x$ crystallizes in the $\text{Mo}_7\text{Sn}_{12}\text{Zn}_{40}$ structure type with a narrow homogeneity range and exhibits metallic behavior with no sign of superconductivity down to at least 1.8 K. Its experimental valence electron count of 2.9 e/atom is below that of endohedral gallium cluster superconductors. Electronic structures of $\text{Mo}_8\text{Ga}_{41-x}\text{Zn}_x$ and $\text{Mo}_7\text{Ga}_{52-x}\text{Zn}_x$ feature the opening of a pseudogap slightly below the Fermi level indicating the specific stability of these structure types at the valence electron count of 3.2 e/atom and 2.7 e/atom, respectively.

1 Introduction

Intermetallic compounds based on gallium often show peculiar transport properties. In contrast to simple metallic-type conductivity seen in many intermetallic phases, the Ga-based intermetallics may show narrow-gap semiconducting behavior or, in some cases, superconducting properties giving rise to new functional materials for the energy conversion, storage, and transfer applications. Ga-based semiconductors include FeGa_3 ¹ ($E_g = 0.5$ eV), RuGa_3 ¹ (0.32 eV), OsGa_3 ² (0.42 eV), and RuGa_2 ³ (0.42 eV). On the other hand, superconducting phases were found in the family of so-called endohedral Ga cluster compounds.⁴ In this family, superconducting $\text{Mo}_8\text{Ga}_{41}$ ⁵ ($T_C = 9.7$ K), $\text{Mo}_6\text{Ga}_{31}$ ⁶

(8 K), $\text{Mo}_4\text{Ga}_{20.5}\text{S}_{0.5}$ ⁷ (5 K), ReGa_5 ⁴ (2.3 K), Rh_2Ga_9 ⁸ (2 K), and Ir_2Ga_9 ⁸ (1.9 K) were reported.

Endohedral Ga cluster superconductors feature crystal structures composed of Ga-based polyhedra with the number of vertices of 8 and higher centered by atoms of a transition metal. In the case of $\text{Mo}_8\text{Ga}_{41}$, $\text{Mo}_6\text{Ga}_{31}$, and $\text{Mo}_4\text{Ga}_{20.5}\text{S}_{0.5}$ phases, the MoGa_{10} polyhedra, which are interconnected by corners, form the structural motif. In the Rh_2Ga_9 and Ir_2Ga_9 compounds, there are the RhGa_9 and IrGa_9 monocapped square antiprisms interconnected through corners and edges. Finally, in ReGa_5 , the ReGa_9 polyhedra share their corners and faces. Within the family of endohedral Ga cluster superconductors, there is a certain correlation between the connectivity of polyhedra, the gross valence electron count (VEC), and the value of superconducting transition temperature.⁴ The transition temperature increases upon moving from the face-sharing and edge-sharing to the solely corner-sharing structures. This correlation is even better defined when the VEC is taken into account. Assuming the total number of valence electrons per one atom in the formula unit, Rh_2Ga_9 and Ir_2Ga_9 with the VEC = 4.1 e/atom are close to semiconducting intermetallics, such as FeGa_3 and RuGa_2 , that usually possess

^a Department of Chemistry, Lomonosov Moscow State University, 119991 Moscow, Russia. E-mail: valeriy.verchenko@gmail.com

^b National Institute of Chemical Physics and Biophysics, 12618 Tallinn, Estonia.

^c Experimental Physics VI, Center for Electronic Correlations and Magnetism, Institute of Physics, University of Augsburg, 86135 Augsburg, Germany.

^d Department of Chemistry, University at Albany, SUNY, Albany, 12222 New York, United States.

[†] Electronic Supplementary Information (ESI) available: X-ray crystallographic files in CIF format. See DOI: 10.1039/b000000x/

VEC > 4. Hence, Rh_2Ga_9 and Ir_2Ga_9 display the lowest transition temperatures in the series. Upon reducing the VEC to 3.7 e/atom (ReGa_5 and $\text{Mo}_4\text{Ga}_{20.5}\text{S}_{0.5}$) and then to 3.5 e/atom ($\text{Mo}_6\text{Ga}_{31}$ and $\text{Mo}_8\text{Ga}_{41}$), the transition temperature substantially increases reaching $T_C \sim 10$ K in the case of $\text{Mo}_8\text{Ga}_{41}$. Interestingly, $\text{Mo}_8\text{Ga}_{41}$ is a strongly coupled superconductor⁹ showing hints for multiband superconductivity.^{10,11} This fact motivates the search for new Ga-cluster superconductors as well as for the study of their superconducting-state properties.

Apparently, the valence electron count plays a crucial role in stability and critical properties of endohedral Ga cluster superconductors. From the experimental point of view, the VEC can be adjusted by the incorporation of two aliovalent metals within one compound.¹² Based on the flux-growth technique, we use the ternary Mo-Ga-Zn flux with excess of Ga and Zn metals to control the gross valence electron count through the Ga/Zn ratio assuming that Ga has three valence electrons, whereas Zn supplies two $4s$ electrons. Starting from $\text{Mo}_8\text{Ga}_{41}$, which can be obtained from the Ga-based flux, we introduce Zn gradually decreasing the gross number of valence electrons and searching for crystallization of new compounds. In this study, we report changes in the crystal structure and transport properties that occur as a result of the Zn for Ga substitution in $\text{Mo}_8\text{Ga}_{41}$, and describe synthesis, crystal structure, and properties of $\text{Mo}_7\text{Ga}_{52-x}\text{Zn}_x$, which was structurally characterized before.¹³ The $\text{Mo}_7\text{Ga}_{52-x}\text{Zn}_x$ compound is closely related to endohedral Ga cluster intermetallics, but shows the reduced VEC. We discuss the evolution of crystal and electronic structures as well as physical properties of the Mo-Ga-Zn compounds upon tuning the VEC parameter.

2 Experimental

Crystal growth was performed using the flux-growth method from the high-temperature ternary Mo-Ga-Zn melt with a variable Ga/Zn ratio. Mo (powder, 99.99%, Merck), Ga (ingots, 5N), and Zn (ingots, 5N) were used as starting reagents. They were weighed in the molar ratio of $v(\text{Mo}):v(\text{Ga}):v(\text{Zn}) = 1 : 50(1 - y) : 50y$ ($y = 0.1; 0.2; 0.3; 0.4; 0.5; 0.6; 0.625; 0.65; 0.675; 0.7; 0.8; 0.9$) and placed inside quartz ampules, which were evacuated to the residual pressure of 5×10^{-3} mbar and sealed. The ampules were placed in a programmable furnace and heated to 1273 K at the rate of 200 K/h, annealed at 1273 K for 2 days, slowly cooled to 673 K at the rate of 4 K/h, and finally cooled to room temperature in the shutoff regime. After this temperature program, the obtained ingots were placed on the top of quartz wool inside quartz ampules, which were evacuated and sealed. The ampules were re-heated to temperatures between 373 K and 723 K depending on the content of Zn in the flux and subsequently transferred to an EBA 280 centrifuge to remove the excess of Ga and Zn metals. The obtained crystals were additionally cleaned from the traces of Ga and Zn metals by 2M HCl and were washed with distilled water and acetone.

Crystals were analyzed on a scanning electron microscope JSM JEOL 6490-LV (30 kV accelerating voltage, secondary electron emission detector) equipped with an energy-dispersive X-ray (EDX) analysis system INCA x-Sight. Elemental mapping with the spatial resolution of $1 \mu\text{m}^2$ was used to determine the distribu-

tion of the elements across the crystal surface. For quantitative analysis, point EDX spectra were recorded and statistically averaged. The point spectra were calibrated using the Mo, GaP, and Zn external standards (MAC Analytical). Further, the crystals were ground, and the resulting powders were analyzed on a Guinier camera Huber G670 [Cu radiation, $\lambda = 1.5406 \text{ \AA}$, Ge (111) monochromator]. Rietveld refinements against the powder X-ray diffraction data (PXRD) were conducted in Jana2006 program¹⁴ using the atomic form factors for Mo and Ga species only. For $\text{Mo}_8\text{Ga}_{41-x}\text{Zn}_x$, details on data collection and structure refinement are presented in Table1, atomic coordinates and displacement parameters are shown in Table2, and selected interatomic distances are listed in Table3.

Single crystals of $\text{Mo}_7\text{Ga}_{52-x}\text{Zn}_x$ were studied on a Bruker D8 Venture single-crystal X-ray diffractometer (Mo radiation, $\lambda = 0.71073 \text{ \AA}$, graphite monochromator). The absorption correction was performed numerically. The crystal structure was determined by the charge-flipping algorithm using the Superflip program.¹⁵ The structure was refined in the full-matrix anisotropic approximation against $|F^2|$ using the SHELXL-2018/3 program.¹⁶ Since Ga and Zn atoms are not distinguishable in the X-ray diffraction experiments, the crystallographic positions of Ga/Zn atoms were refined as jointly populated using equal and fixed occupancy factors, which were taken on the basis of the EDX results. Details on data collection and structure refinement are listed in Table4. The atomic parameters and selected interatomic distances are given in Tables5 and 6, respectively. Crystal structures were visualized using the VESTA program.¹⁷

Electronic structures were calculated within the local density approximation¹⁸ (LDA) of the density-functional theory (DFT) using the full-potential FPLO code¹⁹ (version 14.00-47) with the basis set of local orbitals. Integrations in the k -space were performed by the improved tetrahedron method²⁰ on a grid of $12 \times 12 \times 12$ k -points in the scalar relativistic regime. The virtual crystal approximation (VCA) was used to model the mixing of Ga and Zn atoms.

Electrical resistance was measured on rectangular-shaped pellets with typical dimensions of $8 \times 3 \times 2 \text{ mm}^3$. The pellets were pressed from the crushed crystals at room temperature at the external pressure of 4 kbar. For the four-probe measurements, Cu wires with the diameter of $80 \mu\text{m}$ were attached to pellets using silver-containing epoxy resin (Epotek H20E). Electrical resistance was measured in the temperature range of 2-300 K in zero magnetic field using the Resistivity option of a Physical Properties Measurement System (PPMS, Quantum Design). Magnetization measurements were performed on pieces of the pellets used for electrical resistance measurements. Thereto, a Magnetic Properties Measurement System (MPMS 3 SQUID, Quantum Design) was used, and the measurements were conducted in the zero-field-cooling (*zfc*) and field-cooling (*fc*) conditions at temperatures between 1.8 K and 10 K in the magnetic field of 5 Oe. Magnetization was measured in the *zfc* conditions at 1.8 K by sweeping magnetic field from 0 T to 2 T. Heat capacity was measured on a collection of crystals glued together using a relaxation-type calorimeter (HC option of PPMS, Quantum Design) at temperatures between 1.8 K and 50 K in zero magnetic field.

Table 1 Data collection and refinement details for $\text{Mo}_8\text{Ga}_{41-x}\text{Zn}_x$ [$x = 11.3(2)$].

Parameter	Value
composition, molecular weight (g mol^{-1})	$\text{Mo}_8\text{Ga}_{29.7}\text{Zn}_{11.3}$, 3577.17
composition from EDXS, x	11.3(2)
diffractometer	Guinier camera Huber G670
detector	Image Plate
radiation	$\text{Cu K}\alpha_1$
wavelength (\AA)	1.5406
temperature (K)	300
crystal system	trigonal
space group	$R\bar{3}$ (# 148)
unit cell parameters (\AA)	$a = 14.01884(7)$, $c = 15.05418(9)$
unit cell volume (\AA^3)	2562.19(2)
Z	3
ρ_{calc} (g cm^{-3})	7.05
μ (mm^{-1})	57.99
2θ range (deg)	3–100.3
number of refined parameters	55
R_p	0.0312
R_{wp}	0.0410
R/wR (all data)	0.0267/0.0372
goodness-of-fit	1.71
residual density (e \AA^{-3})	1.02/−0.91

3 Results and discussion

3.1 $\text{Mo}_8\text{Ga}_{41-x}\text{Zn}_x$

$\text{Mo}_8\text{Ga}_{41}$ can be obtained from the Ga-based flux using the synthetic conditions reported previously.⁹ In the current study, we used the joint flux technique¹² to synthesize the Zn-substituted $\text{Mo}_8\text{Ga}_{41-x}\text{Zn}_x$ phase, which was obtained by slow cooling of the $\text{Mo}(\text{Ga}_{1-y}\text{Zn}_y)_{50}$ melt with $0 < y < 0.5$ in the form of submillimeter-size single crystals. PXRD patterns of the crushed crystals show no impurities for $0 < y < 0.5$, and all patterns can be indexed in the trigonal R -centered unit cell. The obtained lattice parameters are shown in Figure 1 as a function of x in $\text{Mo}_8\text{Ga}_{41-x}\text{Zn}_x$, where x was determined by EDX spectroscopy. The a lattice parameter decreases with increasing x in agreement with the fact that the atomic radius of Zn is slightly smaller than that of Ga. The c parameter first goes through a minimum and then slightly increases. The decrease of the a parameter and the simultaneous increase of c cancel each other for $x > 7$ yielding almost constant unit cell volume of this non-Vegard-type solid solution. At the limiting composition of $x = 11.3(2)$, $\text{Mo}_8\text{Ga}_{41-x}\text{Zn}_x$ possesses the unit cell parameters of $a = 14.01885(7)$ \AA and $c = 15.05419(9)$ \AA .

Rietveld refinement of the PXRD pattern (Fig. 1) revealed that $\text{Mo}_8\text{Ga}_{41-x}\text{Zn}_x$ is isomorphous to the parent compound $\text{Mo}_8\text{Ga}_{41}$. The crystal structure of $\text{Mo}_8\text{Ga}_{41-x}\text{Zn}_x$ contains two crystallographic positions for Mo atoms. Mo1 and Mo2 possess the same coordination polyhedron, $\text{Mo}(\text{Ga}/\text{Zn})_{10}$, which is shown in Figure 2a. At the same time, there is a special crystallographic position, namely Ga9, occupied by Ga and Zn atoms, which has no contacts with Mo atoms. Thus, the $(\text{Ga}/\text{Zn})(\text{Ga}/\text{Zn})_{12}$ cuboctahedron is formed around the Ga9 position (Fig. 2b). The Zn

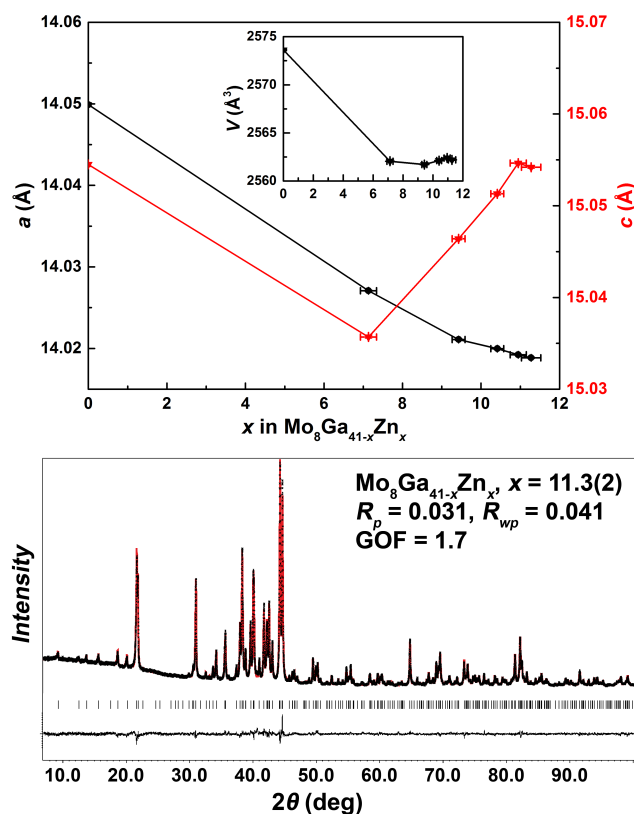


Fig. 1 (Top) Unit cell parameters of $\text{Mo}_8\text{Ga}_{41-x}\text{Zn}_x$ as a function of x . The inset shows the unit cell volume as a function of x . (Bottom) PXRD pattern of the sample with $x = 11.3(2)$. Experimental data are shown by black points, and the calculated pattern is drawn by red line. Peak positions are given by black ticks, and the difference plot is shown by black line in the bottom.

for Ga substitution naturally leads to shortening of most of the interatomic distances (Table 3). As a result, the $\text{Mo}(\text{Ga}/\text{Zn})_{10}$ polyhedra and $(\text{Ga}/\text{Zn})(\text{Ga}/\text{Zn})_{12}$ cuboctahedra are compressed in the crystal structure of $\text{Mo}_8\text{Ga}_{41-x}\text{Zn}_x$. Notably, the distances between Mo atoms and Ga/Zn atoms that form the $(\text{Ga}/\text{Zn})(\text{Ga}/\text{Zn})_{12}$ cuboctahedron, namely Mo1–Ga7, Mo1–Ga8, and Mo2–Ga7, are increased in $\text{Mo}_8\text{Ga}_{41-x}\text{Zn}_x$ indicating the weakened bonding between these atoms. This feature is likely related to the formation of Zn_{13} cuboctahedron clusters centered at the Ga9 crystallographic position, since Zn atoms are effectively less attractive to Mo atoms than Ga. Similar situation has already been observed in the isomorphous compounds $\text{V}_8\text{Ga}_{41-x}\text{Zn}_x$, $\text{Cr}_8\text{Ga}_{41-x}\text{Zn}_x$, and $\text{Mn}_8\text{Ga}_{41-x}\text{Zn}_x$.²¹

Electrical transport measurements indicate the metallic-type behavior of $\text{Mo}_8\text{Ga}_{41-x}\text{Zn}_x$ for $x = 11.3(2)$ (Fig. 3). Resistivity decreases almost linearly with decreasing temperature as expected for a metallic system. The small residual-resistance-ratio (RRR) of 3.5 is probably related to the polycrystalline nature of the sample and to the inherent disorder in the real structure owing to mixed Ga/Zn positions. Measurements on the samples with $x = 7.2(2)$ and $x = 9.5(1)$ show gradual suppression of superconductivity in the system. For $x = 7.2(2)$, the onset of superconductivity is located at $T_C = 4$ K compared to $T_C = 9.8$ K in $\text{Mo}_8\text{Ga}_{41}$,⁹ and the

*Distances for $\text{Mo}_8\text{Ga}_{41}$ were obtained from the Rietveld refinement of the respective PXRD pattern ($R_p = 0.0393$, $R_{wp} = 0.0504$, $R_{all} = 0.0257$, $wR_{all} = 0.0408$, $\text{GOF} = 2.15$).

†Occupancies of the Ga1–Ga8 positions are fixed to $0.4615\text{Ga} + 0.5385\text{Zn}$.

Table 2 Atomic coordinates and displacement parameters for $\text{Mo}_8\text{Ga}_{41-x}\text{Zn}_x$ [$x = 11.3(2)$].

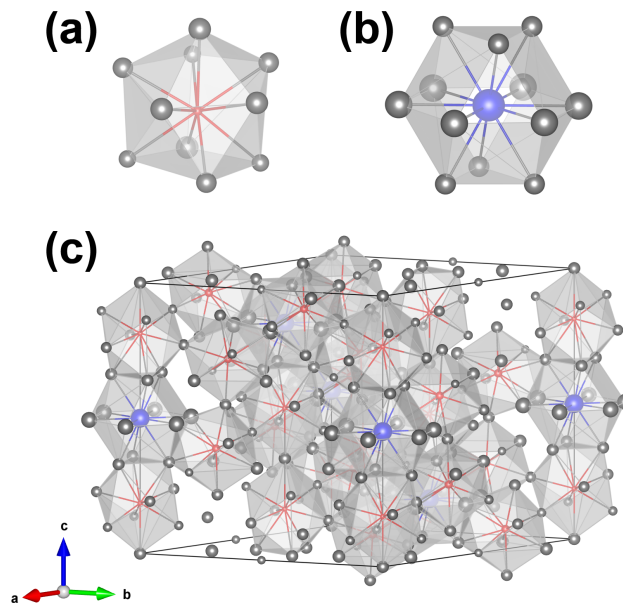
Atom	Site	x	y	z	U_{iso} (\AA^2)
Mo1	18f	0.03213(9)	0.35009(9)	0.0676(1)	0.0067(3)
Mo2	6c	0	0	0.1864(1)	0.0027(6)
Ga1	18f	0.0105(2)	0.1674(2)	0.1128(1)	0.0085(5)
Ga2	18f	0.1772(2)	0.1802(2)	0.2201(1)	0.0117(6)
Ga3	18f	0.3202(1)	0.0081(2)	0.2321(1)	0.0132(5)
Ga4	18f	0.3257(1)	0.1420(2)	0.0038(1)	0.0157(6)
Ga5	9e	0.5	0	0	0.0068(7)
Ga6	3a	0	0	0	0.014(1)
Ga7	18f	0.1202(1)	0.0062(2)	0.3425(1)	0.0141(5)
Ga8	18f	0.2232(2)	0.4300(1)	0.1654(2)	0.0242(5)
Ga9	3b	0	0	0.5	0.034(2)

Table 3 Selected interatomic distances (\AA) in the crystal structures of $\text{Mo}_8\text{Ga}_{41-x}\text{Zn}_x$ [$x = 11.3(2)$] and $\text{Mo}_8\text{Ga}_{41}$.*

Bond	$\text{Mo}_8\text{Ga}_{41-x}\text{Zn}_x$	$\text{Mo}_8\text{Ga}_{41}$
Mo1–Ga1	2.518(3)	2.627(3)
–Ga2	2.599(3)	2.629(4)
–Ga3	2.537(3)	2.593(4)
–Ga3	2.545(3)	2.560(4)
–Ga4	2.575(2)	2.643(3)
–Ga4	2.552(3)	2.611(4)
–Ga5	2.569(2)	2.553(2)
–Ga7	2.832(2)	2.704(2)
–Ga8	2.756(3)	2.602(3)
–Ga8	2.791(3)	2.716(4)
Mo2–3Ga1	2.532(2)	2.615(3)
–3Ga2	2.556(3)	2.626(4)
–Ga6	2.806(2)	3.013(3)
–3Ga7	2.867(3)	2.652(4)
Ga9–6Ga7	2.884(2)	2.968(3)
–6Ga8	2.875(2)	2.924(4)

zero resistance is found at temperatures below 3 K. The bulk nature of superconductivity in $\text{Mo}_8\text{Ga}_{41-x}\text{Zn}_x$ with $x = 7.2(2)$ is confirmed by thermodynamic measurements. The dimensionless volume magnetic susceptibility measured in 5 Oe magnetic field exhibits the strong diamagnetic shift below $T_C = 4$ K both in the zfc and fc conditions. The zfc signal of $4\pi\chi_V$ reaches the value of -1.4 at $T = 1.8$ K suggesting a large volume fraction of the superconducting phase. The volume magnetization measured at $T = 1.8$ K in the zfc conditions also shows the diamagnetic shift characteristic of a type-II superconductor. Heat capacity of $\text{Mo}_8\text{Ga}_{41-x}\text{Zn}_x$ with $x = 7.2(2)$ measured in zero magnetic field exhibits the broad maximum below $T_C \sim 4$ K confirming the bulk nature of superconductivity. It should be noted, however, that no clear heat-capacity anomaly is visible, as well as the transition to the superconducting state is significantly broadened with temperature according both to the heat-capacity and magnetization measurements. Presumably, this broadening is caused by the Ga/Zn disorder in the real structure of $\text{Mo}_8\text{Ga}_{41-x}\text{Zn}_x$.

For $x = 9.5(1)$, only the onset of superconductivity located at $T_C = 2.5$ K is visible in the resistivity curve. Measurements below 2 K would be required to test the bulk nature of superconductivity in this sample. In the $x = 11.3(2)$ sample, no signatures of superconductivity were observed down to 1.8 K suggesting further suppression of the superconducting transition. On one hand, the suppression of superconductivity may be caused by the disorder introduced by the Zn for Ga substitution. On the other hand, the VEC of $\text{Mo}_8\text{Ga}_{41-x}\text{Zn}_x$ is significantly reduced: compared to

**Fig. 2** Crystal structure of $\text{Mo}_8\text{Ga}_{41-x}\text{Zn}_x$: (a) $\text{Mo}(\text{Ga}/\text{Zn})_{10}$ polyhedron; (b) $(\text{Ga}/\text{Zn})(\text{Ga}/\text{Zn})_{12}$ cuboctahedron centered at the Ga9 crystallographic position; (c) unit cell content. Mo atoms are shown in red, Ga and Zn in grey, and the Ga9 crystallographic position in blue.

$\text{Mo}_8\text{Ga}_{41}$ with the VEC = 3.5 e/atom, $\text{Mo}_8\text{Ga}_{41-x}\text{Zn}_x$ possesses 3.3 e/atom for its limiting composition of $x = 11.3(2)$. It is hard to predict how the superconducting transition temperature depends on the valence electron count in the family of endohedral Ga cluster superconductors. However, the dome-like behavior was proposed with a maximum at $T_C \sim 10$ K for $\text{Mo}_8\text{Ga}_{41}$ and the absence of superconductivity at lower values of the VEC.⁴ At this point, our results extend the proposed picture, since we documented the superconductivity of $\text{Mo}_8\text{Ga}_{41-x}\text{Zn}_x$ with $x = 7.2(2)$ and VEC = 3.34 e/atom at $T_C = 4$ K in zero magnetic field.

3.2 $\text{Mo}_7\text{Ga}_{52-x}\text{Zn}_x$

By further increasing the Zn content in the joint flux, the $\text{Mo}_7\text{Ga}_{52-x}\text{Zn}_x$ compound can be reached. It is obtained from the $\text{Mo}(\text{Ga}_{1-y}\text{Zn}_y)_{50}$ melt with $0.625 < y < 0.675$ as a single-phase product in the form of millimeter-size cubic crystals. The single-phase nature of the samples was confirmed by PXRD (Fig.4). According to the EDX spectroscopy, $\text{Mo}_7\text{Ga}_{52-x}\text{Zn}_x$ possesses a narrow homogeneity range of $28.0(4) < x < 33.1(5)$. The selected

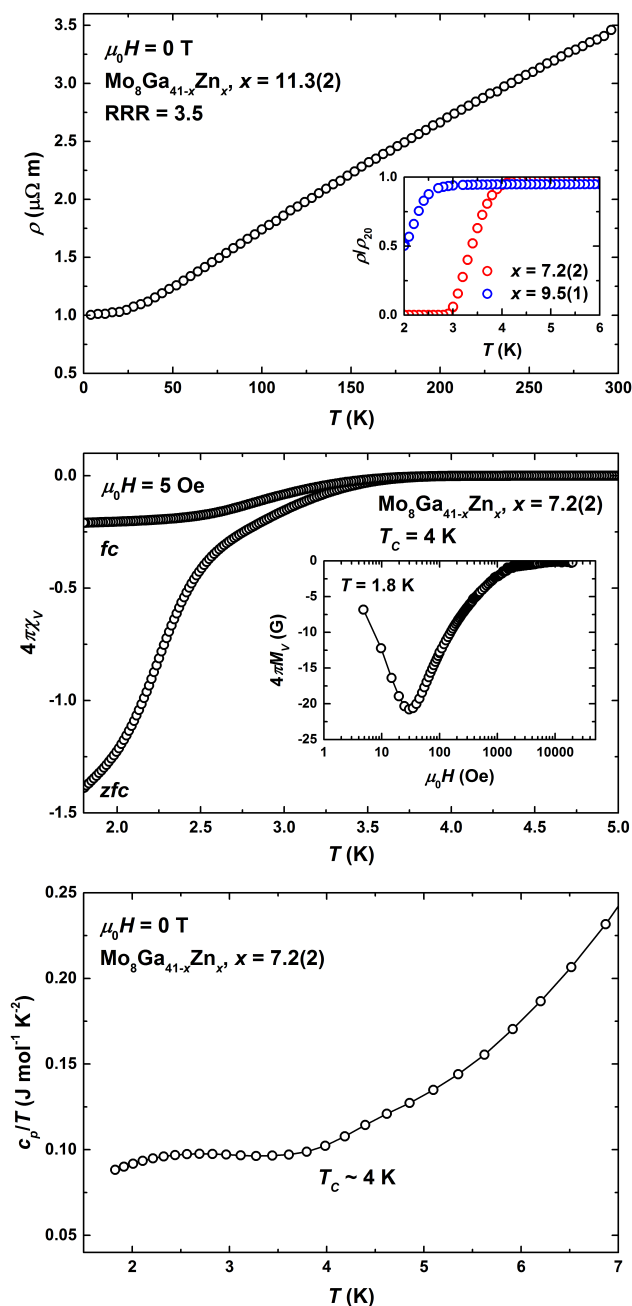


Fig. 3 (Top) Resistivity of $\text{Mo}_8\text{Ga}_{41-x}\text{Zn}_x$ with $x = 11.3(2)$ as a function of temperature in zero magnetic field. The inset shows the low-temperature zero-field resistivity of $\text{Mo}_8\text{Ga}_{41-x}\text{Zn}_x$ with $x = 7.2(2)$ (red circles) and $x = 9.5(1)$ (blue circles). (Middle) Dimensionless volume magnetic susceptibility of $\text{Mo}_8\text{Ga}_{41-x}\text{Zn}_x$ with $x = 7.2(2)$ measured in the *zfc* and *fc* conditions in the magnetic field of 5 Oe. The inset shows the volume magnetization measured at 1.8 K. (Bottom) Heat capacity of $\text{Mo}_8\text{Ga}_{41-x}\text{Zn}_x$ with $x = 7.2(2)$ in zero magnetic field plotted as c_p/T vs T .

single crystals with $x = 28.0(4)$ were studied by the single-crystal X-ray diffraction, and the collected data were indexed in the *F*-centered cubic unit cell with $a = 24.813(1)$ Å. The *Fm-3c* space group (# 226) was chosen on the basis of diffraction pattern symmetry and systematic extinction conditions. Subsequent structure solution and refinement showed that the compound is isomor-

Table 4 Data collection and structure refinement parameters for $\text{Mo}_7\text{Ga}_{52-x}\text{Zn}_x$ [$x = 28.0(4)$].

Parameter	Value
composition, molecular weight (g mol^{-1})	$\text{Mo}_7\text{Ga}_{24}\text{Zn}_{28}$, 4175.642
composition from EDXS, x	28.0(4)
crystal dimensions (μm)	$133 \times 97 \times 96$
diffractometer	Bruker D8 Venture
detector	Photon 100 CMOS
radiation	Mo K_α
wavelength (Å)	0.71073
scan mode	ω/θ
temperature (K)	100
crystal system	cubic
space group	<i>Fm-3c</i> (# 226)
unit cell parameters (Å)	$a = 24.813(1)$
unit cell volume (Å ³)	15278(2)
Z	16
ρ_{calc} (g cm^{-3})	7.26
μ (mm^{-1})	35.97
θ_{max} (deg)	36.29
<i>hkl</i> ranges	$-40 \leq h \leq 41$, $-36 \leq k \leq 36$, $-41 \leq l \leq 37$
No. of measured/independent reflections	30646/1642
No. of reflections with $I > 2\sigma(I)$	1401
R_{int}	0.0893
absorption correction	numerical
transmission coefficients $t_{\text{min}}/t_{\text{max}}$	0.0955/0.1626
No. of parameters	54
R_1/wR_2 [$I > 2\sigma(I)$]	0.0342/0.0583
R_1/wR_2 (all data)	0.0481/0.0608
goodness-of-fit	1.21
residual density ($\text{e} \text{ \AA}^{-3}$)	1.376/-2.983

phous to $\text{Mo}_7\text{Sn}_{12}\text{Zn}_{40}$ being just the second representative of this rare structure type.²²

In the crystal structure of $\text{Mo}_7\text{Ga}_{52-x}\text{Zn}_x$, there are three Mo positions and eight positions mutually occupied by Ga/Zn atoms. Coordination polyhedra of the Mo1, Mo2, and Mo3 atoms are shown in Figure 5a-c, respectively. In contrast to the complex and distorted $\text{Mo}(\text{Ga}/\text{Zn})_{10}$ polyhedra found in the crystal structure of $\text{Mo}_8\text{Ga}_{41-x}\text{Zn}_x$ (Fig. 2a), Mo atoms in $\text{Mo}_7\text{Ga}_{52-x}\text{Zn}_x$ possess a highly symmetric environment. Mo1 and Mo3 atoms are located inside the $(\text{Ga}/\text{Zn})_{12}$ icosahedra, whereas the Mo2 atoms are placed inside the $(\text{Ga}/\text{Zn})_{14}$ rhombic dodecahedra. In the *F*-centered cubic unit cell, the Mo1(Ga/Zn)₁₂ icosahedra are located at the corners, at the centers of edges and faces, and in the middle of the unit cell dividing it into eight octants (Fig. 5d). Each octant is centered by the Mo2(Ga/Zn)₁₄ rhombic dodecahedron (Fig. 5e). A closer look at the octant reveals an elegant arrangement: the Mo2(Ga/Zn)₁₄ rhombic dodecahedron is placed inside a $(\text{Ga}/\text{Zn})_{24}$ snub cube formed by Ga/Zn atoms that belong to the Ga1 position (Fig. 5f). The Mo3(Ga/Zn)₁₂ icosahedra share their vertices with the $(\text{Ga}/\text{Zn})_{24}$ snub cube forming a supercuboctahedron, which completes the inner part of the octant (Fig. 5g). Finally, eight octants with the Mo1(Ga/Zn)₁₂ icosahedra in the corners are combined forming a unit cell of the $\text{Mo}_7\text{Ga}_{52-x}\text{Zn}_x$ crystal structure, which is shown in Figure 5h.

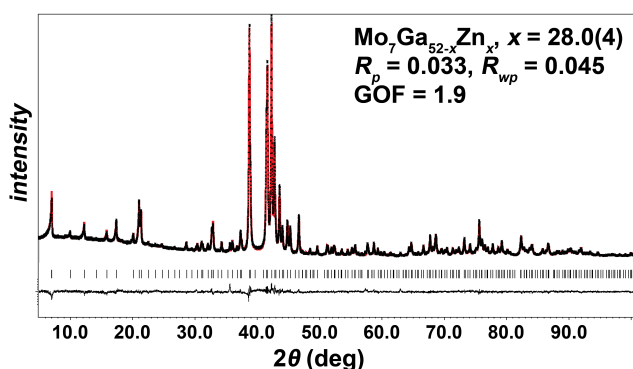
As was mentioned above, $\text{Mo}_7\text{Ga}_{52-x}\text{Zn}_x$ is isomorphous to the $\text{Mo}_7\text{Sn}_{12}\text{Zn}_{40}$ approximant phase.²² Recently, the $\text{Cr}_{22}\text{Zn}_{72}\text{Sn}_{24}$ complex intermetallic phase, which is closely related to the $\text{Mo}_7\text{Ga}_{52-x}\text{Zn}_x$ and $\text{Mo}_7\text{Sn}_{12}\text{Zn}_{40}$ compounds, was discovered in

Table 5 Atomic coordinates and displacement parameters for $\text{Mo}_7\text{Ga}_{52-x}\text{Zn}_x$ [$x = 28.0(4)$].

Atom	Site	x	y	z	U_{eq} (\AA^2)
Mo1	8b	0	0	0	0.0018(3)
Mo2	8a	1/4	1/4	1/4	0.0012(3)
Mo3	96i	0	0.11208(2)	0.17773(2)	0.00149(9)
Ga1 [‡]	192j	0.08610(2)	0.16477(2)	0.20593(2)	0.0053(1)
Ga2	48e	0.18042(4)	0	0	0.0042(2)
Ga3	96i	0	0.05687(3)	0.08928(3)	0.0018(1)
Ga4	192j	0.06038(2)	0.14953(2)	0.09453(2)	0.00352(9)
Ga5	96i	0	0.22087(3)	0.15681(3)	0.0040(1)
Ga6	96h	1/4	0.06031(2)	y	0.0026(1)
Ga7	64g	0.18667(2)	x	x	0.0051(2)
Ga8	48f	0.12905(4)	1/4	1/4	0.0059(2)

Table 6 Selected interatomic distances in the crystal structure of $\text{Mo}_7\text{Ga}_{52-x}\text{Zn}_x$ [$x = 28.0(4)$].

Bond	Distance (\AA)
Mo1–12Ga3	2.6266(7)
Mo2–8Ga7	2.7219(8)
–4Ga8	3.001(1)
Mo3–2Ga4	2.7149(7)
–2Ga4	2.7634(6)
–Ga2	2.7818(5)
–Ga3	2.5871(8)
–2Ga1	2.6009(6)
–2Ga6	2.6656(4)
–2Ga5	2.7501(9)

**Fig. 4** Experimental (black points) and calculated (red line) PXRD patterns of $\text{Mo}_7\text{Ga}_{52-x}\text{Zn}_x$ with $x = 28.0(4)$. Positions of peaks are shown by black ticks, and the difference plot is presented as a black line in the bottom.

the Cr-Zn-Sn ternary system.²³ $\text{Cr}_{22}\text{Zn}_{72}\text{Sn}_{24}$ crystallizes in the $Fm\text{-}3c$ space group (# 226) and possesses similar lattice parameter, a , and exactly the same total number of atoms per unit cell. Moreover, the crystal structure of $\text{Cr}_{22}\text{Zn}_{72}\text{Sn}_{24}$ has almost the same pattern except the fact that Cr atoms locate not only in the center of a rhombic dodecahedron unit but also in its vertices resulting in higher content of Cr per formula unit when compared to $\text{Mo}_7\text{Ga}_{52-x}\text{Zn}_x$.

Comparing $\text{Mo}_7\text{Ga}_{52-x}\text{Zn}_x$ to $\text{Mo}_8\text{Ga}_{41-x}\text{Zn}_x$, one notes that in both structures the Mo-based polyhedra are interconnected by corners. The principal difference between the structures of $\text{Mo}_8\text{Ga}_{41-x}\text{Zn}_x$ and $\text{Mo}_7\text{Ga}_{52-x}\text{Zn}_x$ is that the former contains the special position of Ga/Zn atoms that are bonded solely to other Ga/Zn atoms, while the latter structure does not feature such site. In the crystal structure of $\text{Mo}_7\text{Ga}_{52-x}\text{Zn}_x$, all Ga/Zn atoms belong

to either of the Mo1, Mo2, and Mo3-based polyhedra.

Electrical resistivity of $\text{Mo}_7\text{Ga}_{52-x}\text{Zn}_x$ with $x = 28.0(4)$ decreases with decreasing temperature, thus indicating the metallic behavior (Fig.6). The small value of RRR = 1.25 as well as the slight upturn of the resistivity curve at low temperatures may appear due to disorder in the crystal structure caused by the mixing of Ga and Zn atoms. Similar to $\text{Mo}_8\text{Ga}_{41-x}\text{Zn}_x$ with $x = 11.3(2)$, no superconducting anomaly is present at temperatures above 2 K in zero magnetic field. Low-temperature zero-field measurements of the heat capacity corroborate these results and show the absence of any phase transition above 1.8 K. The low-temperature heat capacity was fitted using the equation $c_p = \gamma T + \beta T^3$ yielding $\gamma = 42.8(2)$ mJ mol⁻¹ K⁻² and $\beta = 2.63(2)$ mJ mol⁻¹ K⁻⁴. The value of β corresponds to the Debye temperature of $\Theta_D = 352$ K. The obtained value of the Sommerfeld coefficient indicates a noticeable contribution of the conduction electrons to the total heat capacity in agreement with the metallic behavior deduced from the resistivity measurements.

3.3 Electronic structures

As it was already mentioned, $\text{Mo}_8\text{Ga}_{41-x}\text{Zn}_x$ possesses the VEC = 3.3 e/atom for its limiting composition of $x = 11.3(2)$. In $\text{Mo}_7\text{Ga}_{52-x}\text{Zn}_x$ with $x = 28.0(4)$, the VEC is further reduced reaching the value of 2.9 e/atom. In order to clarify whether the reduction of VEC on going from $\text{Mo}_8\text{Ga}_{41-x}\text{Zn}_x$ to $\text{Mo}_7\text{Ga}_{52-x}\text{Zn}_x$ is correlated with stability of the corresponding structure types, electronic structure calculations were performed.

Density of states plots calculated for $\text{Mo}_8\text{Ga}_{41-x}\text{Zn}_x$ ($x = 11.3$) and $\text{Mo}_7\text{Ga}_{52-x}\text{Zn}_x$ ($x = 28$) shown in Figure7 demonstrate similar patterns in both compounds. At low relative energies of -10 eV $< E - E_F < -5$ eV, the density of states is dominantly formed by the 4s and 4p contributions of Ga/Zn. At energies around the Fermi level, -5 eV $< E - E_F < 5$ eV, the 4d Mo states emerge. Their strong hybridization with the Ga/Zn 4p states leads to the formation of a pseudogap near the Fermi energy. In the case of $\text{Mo}_8\text{Ga}_{41-x}\text{Zn}_x$, this pseudogap corresponds to the VEC = 3.2 e/atom, while for $\text{Mo}_7\text{Ga}_{52-x}\text{Zn}_x$, the opening of a pseudogap is observed already at VEC = 2.7 e/atom. In each case, the Fermi level is located slightly above the pseudogap leading to a metallic ground state, which was found experimentally for both compounds. For $\text{Mo}_7\text{Ga}_{52-x}\text{Zn}_x$ with $x = 28$, the density of states at the Fermi energy, $N(E_F) = 18.8$ st. eV⁻¹ f.u.⁻¹, corresponds to the calculated Sommerfeld coefficient of $\gamma_{bare} = 44.3$ mJ mol⁻¹

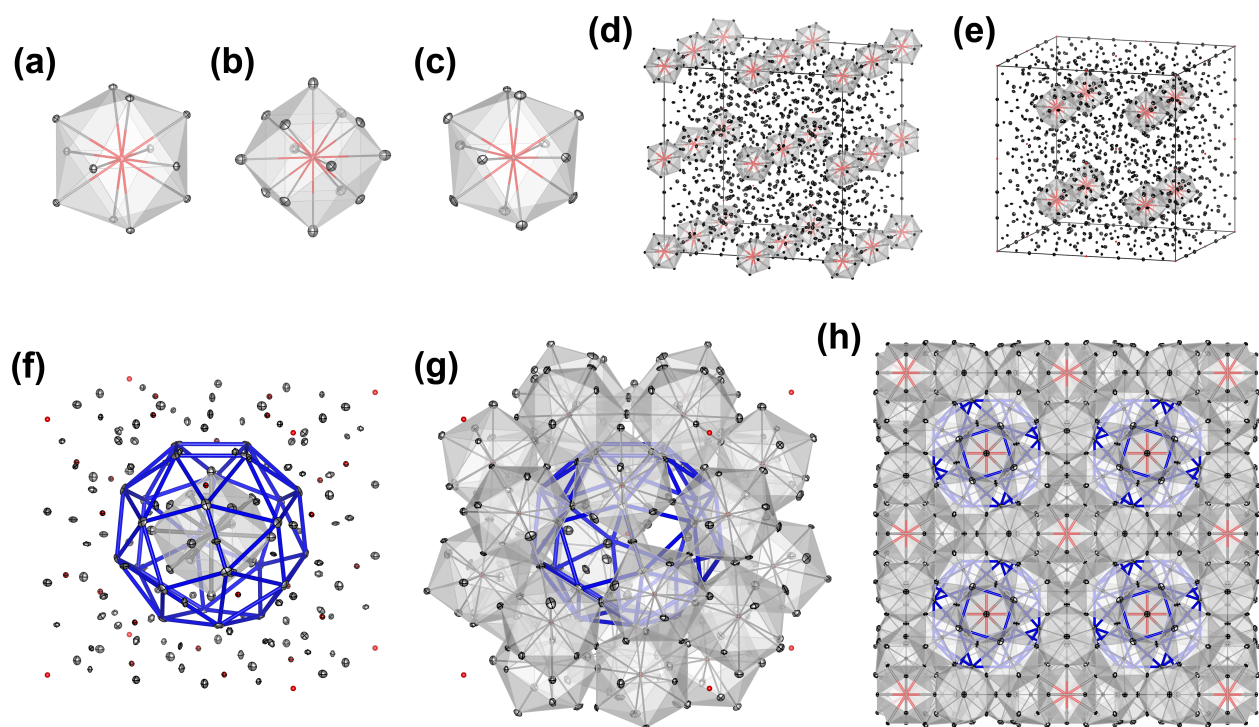


Fig. 5 Crystal structure of $\text{Mo}_7\text{Ga}_{52-x}\text{Zn}_x$: (a-c) coordination polyhedra of the Mo1, Mo2, and Mo3 positions, respectively; (d) arrangement of the $\text{Mo1}(\text{Ga}/\text{Zn})_{12}$ icosahedra in the unit cell; (e) $\text{Mo2}(\text{Ga}/\text{Zn})_{14}$ rhombic dodecahedra in the unit cell; (f) one octant containing a $(\text{Ga}/\text{Zn})_{24}$ snub cube centered by the $\text{Mo2}(\text{Ga}/\text{Zn})_{14}$ rhombic dodecahedron; (g) $\text{Mo3}(\text{Ga}/\text{Zn})_{12}$ icosahedra surrounding the $(\text{Ga}/\text{Zn})_{24}$ snub cube and forming a supercuboctahedron in one octant; (h) eight octants in the unit cell of the $\text{Mo}_7\text{Ga}_{52-x}\text{Zn}_x$ crystal structure. Atoms are shown as displacement ellipsoids on the probability level of 95%. Mo atoms are shown in red, Ga and Zn in grey.

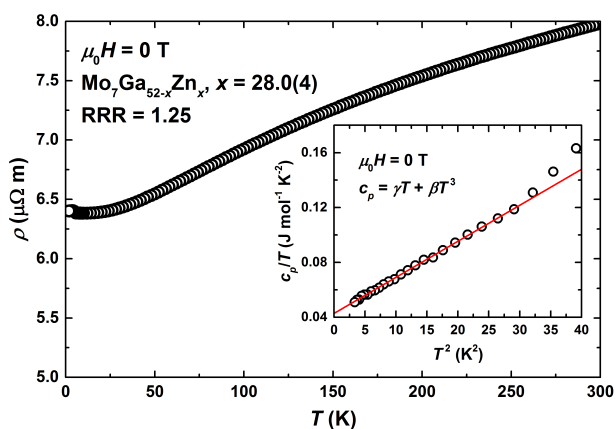


Fig. 6 Electrical resistivity of $\text{Mo}_7\text{Ga}_{52-x}\text{Zn}_x$ [$x = 28.0(4)$] as a function of temperature in zero magnetic field. The inset shows the low-temperature zero-field heat capacity of the same sample plotted as c_p/T vs. T^2 . The solid red line is a least-squares fit of the data.

K^{-2} , which is in good agreement with the experimental value of $\gamma = 42.8(2) \text{ mJ mol}^{-1} \text{ K}^{-2}$.

The electronic structures of both $\text{Mo}_8\text{Ga}_{41-x}\text{Zn}_x$ and $\text{Mo}_7\text{Ga}_{52-x}\text{Zn}_x$ exhibit a special feature: the opening of a pseudogap driven by the hybridization between the Mo $4d$ states and Ga/Zn $4p$ states. The positions of pseudogaps in terms of the VEC define stable electronic configurations of intermetallic struc-

ture types. We argue that both $\text{Mo}_8\text{Ga}_{41-x}\text{Zn}_x$ and $\text{Mo}_7\text{Ga}_{52-x}\text{Zn}_x$ are closely related to polar intermetallic compounds that obey the electron counting rules. For instance, more than 34 binary intermetallic structure types conform to the $18 - n$ rule that predicts the stable electronic configuration depending on n , the number of short contacts between transition-metal atoms.²⁴ However, the $18 - n$ rule as well as the modified $18 - n + m$ rule, which additionally accounts for the bonding between non-transition elements, both fail to explain the VEC values found for $\text{Mo}_8\text{Ga}_{41-x}\text{Zn}_x$ and $\text{Mo}_7\text{Ga}_{52-x}\text{Zn}_x$ in our electronic structure calculations. This problem has already been formulated for the V_8Ga_{41} structure type,²⁴ and it has now emerged for the $\text{Mo}_7\text{Sn}_{12}\text{Zn}_{40}$ -type intermetallics.

The overall decrease in the VEC upon going from $\text{Mo}_8\text{Ga}_{41-x}\text{Zn}_x$ (3.3 e/atom for $x = 11.3$) to $\text{Mo}_7\text{Ga}_{52-x}\text{Zn}_x$ (2.9 e/atom for $x = 28$) reveals the tendency of moving beyond the endohedral cluster compounds and approaching approximant phases and quasicrystals. Indeed, the VEC of $\text{Mo}_7\text{Ga}_{52-x}\text{Zn}_x$ is in between that for Ga cluster superconductors (3.5–4.1 e/atom) and Bergman-type quasicrystals (2.1–2.2 e/atom).²⁵ Accordingly, the crystal structure of $\text{Mo}_7\text{Ga}_{52-x}\text{Zn}_x$ is built by highly symmetric Mo-based polyhedra, namely, the $\text{Mo}(\text{Ga}/\text{Zn})_{12}$ icosahedra and $\text{Mo}(\text{Ga}/\text{Zn})_{14}$ rhombic dodecahedra, which were not found in the crystal structures of endohedral Ga cluster superconductors. The complex yet elegant crystal structure of $\text{Mo}_7\text{Ga}_{52-x}\text{Zn}_x$ originates from the approximant nature of this intermetallic compound.

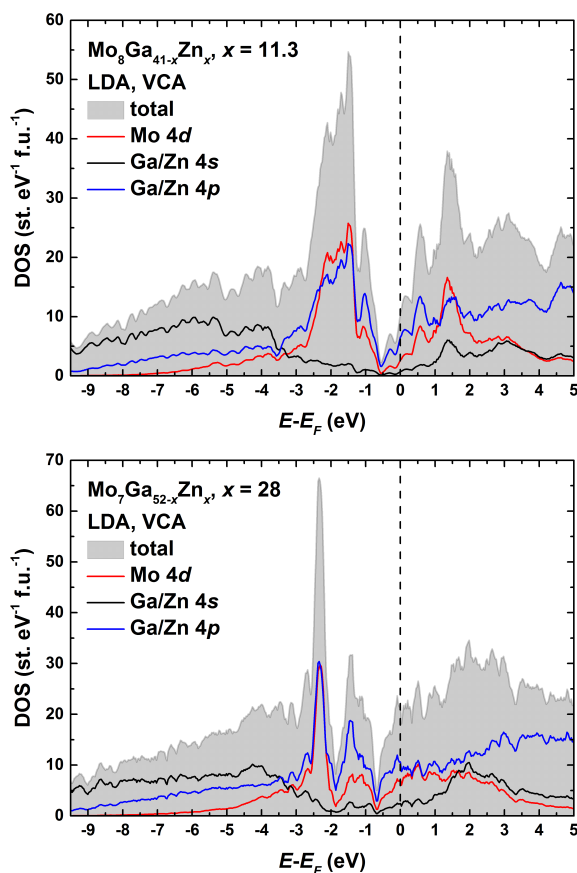


Fig. 7 Density of states plots calculated for $\text{Mo}_8\text{Ga}_{41-x}\text{Zn}_x$ with $x = 11.3$ (top) and $\text{Mo}_7\text{Ga}_{52-x}\text{Zn}_x$ with $x = 28$ (bottom). The Mo 4d, Ga/Zn 4s, and Ga/Zn 4p states are shown by the red, black, and blue lines, respectively. The position of the Fermi level is indicated by the dashed line.

4 Conclusions

By employing crystal growth from the joint flux, we tuned the gross valence electron count in the Mo-Ga-Zn system. As a result, the $\text{Mo}_8\text{Ga}_{41-x}\text{Zn}_x$ and $\text{Mo}_7\text{Ga}_{52-x}\text{Zn}_x$ intermetallic compounds were obtained in the form of high-quality crystals. At first, gradual increase in the Zn content of the flux leads to a decrease of the valence electron count in the $\text{Mo}_8\text{Ga}_{41-x}\text{Zn}_x$ phase through the Zn for Ga substitution, which occurs for $0 \leq x \leq 11.3(2)$, while preserving the parent structure type. Analysis of bond distances reveals possible formation of Zn cuboctahedral clusters in the crystal structure. Electrical resistivity measurements show that superconductivity is gradually suppressed in $\text{Mo}_8\text{Ga}_{41-x}\text{Zn}_x$ when the content of Zn is increased with no sign of superconductivity for the limiting composition of $x = 11.3(2)$ at temperatures above 2 K. By further decreasing the gross number of valence electrons, the $\text{Mo}_7\text{Ga}_{52-x}\text{Zn}_x$ compound was reached. It crystallizes in the $\text{Mo}_7\text{Sn}_{12}\text{Zn}_{40}$ structure type and possesses the narrow homogeneity range of $28.0(4) \leq x \leq 33.1(5)$. $\text{Mo}_7\text{Ga}_{52-x}\text{Zn}_x$ exhibits the metallic behavior for $x = 28.0(4)$ with no sign of superconductivity at temperatures above 1.8 K. Electronic structure calculations reveal the formation of a pseudogap slightly below the Fermi level for both compounds. This pseudogap corresponds to the valence

electron count of 3.2 e/atom and 2.7 e/atom in $\text{Mo}_8\text{Ga}_{41-x}\text{Zn}_x$ and $\text{Mo}_7\text{Ga}_{52-x}\text{Zn}_x$, respectively, indicating that the title compounds are closely related to polar intermetallic compounds, which stability can be explained through the electron counting rules. However, $\text{Mo}_8\text{Ga}_{41-x}\text{Zn}_x$ and $\text{Mo}_7\text{Ga}_{52-x}\text{Zn}_x$ do not adhere to such rules owing to the complex bonding patterns that can not be quantified in terms of simple two-center two-electron bonding. The position of a pseudogap for $\text{Mo}_7\text{Ga}_{52-x}\text{Zn}_x$ at 2.7 e/atom is significantly lower than experimental values of the valence electron count for known endohedral Ga cluster superconductors. This fact places $\text{Mo}_7\text{Ga}_{52-x}\text{Zn}_x$ behind Ga cluster superconductors in terms of the VEC, and triggers similarities to the electron-deficient approximant phases and quasicrystals. This is reflected in the crystal structure of $\text{Mo}_7\text{Ga}_{52-x}\text{Zn}_x$, which is built by highly symmetric coordination polyhedra, namely $\text{Mo}(\text{Ga}/\text{Zn})_{12}$ icosahedra and $\text{Mo}(\text{Ga}/\text{Zn})_{14}$ rhombic dodecahedra, arranged in an elegant way in the *F*-centered cubic unit cell.

Conflicts of interest

The authors declare that they have no conflict of interest.

Acknowledgements

The work is supported by the Russian Science Foundation, Grant No. 17-13-01033. V.Yu.V. is grateful for the financial support from the Mobilitas program of the European Science Foundation, Grant No. MOBJD449. The work in Augsburg was supported by the Federal Ministry for Education and Research under the Sofja Kovalevskaya Award of the Alexander von Humboldt Foundation. E.V.D. thanks the National Science Foundation, Grant No. CHE-1337594.

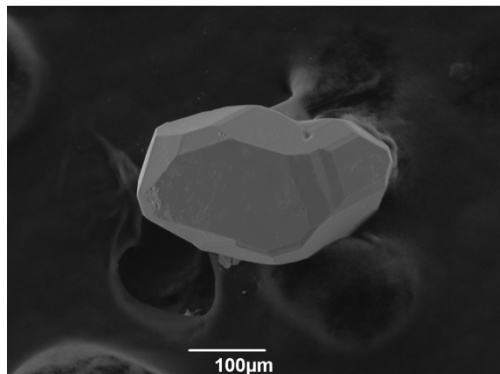
Notes and references

- U. Häussermann, M. Boström, P. Viklund, O. Rapp and T. Björnängen, *J. Solid. State Chem.*, 2002, **165**, 94–99.
- Y. Amagai, A. Yamamoto, T. Lida and Y. Takahashi, *J. Appl. Phys.*, 2004, **96**, 5644.
- J. Evers, G. Oehlinger and H. Meyer, *Mat. Res. Bull.*, 1984, **19**, 1177–1180.
- W. Xie, H. Luo, B. Phelan, T. Klimczuk, F. Cevallos and R. Cava, *Proc. Natl. Acad. Sci. USA*, 2015, **112**, E7048–E7054.
- A. Bezinge, K. Yvon, M. Decroux and J. Muller, *J. Less-Common Met.*, 1984, **99**, L27–L31.
- O. Fisher, *Helvetica Physica Acta*, 1972, **45**, 331.
- M. Wolczyk, R. Andruszkiewicz and K. Lukaszewicz, *Acta Cryst. C*, 1989, **45**, 991–993.
- T. Shibayama, M. Nohara, H. Katori, Y. Okamoto, Z. Hiroi and H. Takagi, *J. Phys. Soc. Jpn.*, 2007, **76**, 073708.
- V. Verchenko, A. Tsirlin, A. Zubtsovskiy and A. Shevelkov, *Phys. Rev. B*, 2016, **93**, 064501.
- V. Verchenko, R. Khasanov, Z. Guguchia, A. Tsirlin and A. Shevelkov, *Phys. Rev. B*, 2017, **96**, 134504.
- P. Neha, P. Sivaprakash, K. Ishigaki, G. Kalaiselvan, K. Manikandan, R. Dhaka, Y. Uwatoko, S. Arumugam and S. Patnaik, *Mater. Res. Express*, 2019, **6**, 016002.

- 12 V. Verchenko, A. Mironov, Z. Wei, A. Tsirlin, E. Dikarev and A. Shevelkov, *Inorg. Chem.*, 2019, **58**, 1561–1570.
- 13 R. Lux, *Dissertation: Intermetallische Verbindungen mit hochschmelzenden Übergangsmetallen und niedrignschmelzenden Metallen*, University of Freiburg, Freiburg, Germany, 2004.
- 14 V. Petříček, M. Dušek and L. Palatinus, *Z. Kristallogr.*, 2014, **229**, 345.
- 15 L. Palatinus and G. Chapuis, *J. Appl. Cryst.*, 2007, **40**, 786–790.
- 16 G. Sheldrick, *Acta Crystallogr., Sect. C: Struct. Chem.*, 2015, **C71**, 3–8.
- 17 K. Momma and F. Izumi, *J. Appl. Cryst.*, 2011, **44**, 1272–1276.
- 18 J. Perdew and Y. Wang, *Phys. Rev. B*, 1992, **45**, 13244.
- 19 K. Koepnik and H. Eschrig, *Phys. Rev. B*, 1999, **59**, 1743.
- 20 P. Blöchl, O. Jepsen and O. Andersen, *Phys. Rev. B*, 1994, **49**, 16223.
- 21 P. Viklund, C. Svensson, S. Hull, S. Simak, P. Berastegui and U. Häussermann, *Chem. Eur. J.*, 2001, **7**, 5143–5152.
- 22 H. Hillbrecht, V. Kuntze and K. Gebhardt, *Z. Kristallogr.*, 1997, **212**, 840–847.
- 23 W. Xie, R. Cava and G. Miller, *J. Mater. Chem. C*, 2017, **5**, 7215–7221.
- 24 V. Yannello and D. Fredrickson, *Inorg. Chem.*, 2015, **54**, 11385–11398.
- 25 V. Smetana, Q. Lin, D. Pratt, A. Kreyssig, M. Ramazanoglu, J. Corbett, A. Goldman and G. Miller, *Angew. Chem. Int. Ed.*, 2012, **51**, 12699–12702.

By employing the joint flux technique, the gross valence electron count has been adjusted in the Mo-Ga-Zn ternary system yielding the $\text{Mo}_8\text{Ga}_{41-x}\text{Zn}_x$ and $\text{Mo}_7\text{Ga}_{52-x}\text{Zn}_x$ intermetallic compounds.

$\text{Mo}_8\text{Ga}_{41-x}\text{Zn}_x$
VEC ~ 3.3 e/atom



$\text{Mo}_7\text{Ga}_{52-x}\text{Zn}_x$
VEC ~ 2.9 e/atom

